

Raman Scattering Study of Lattice Vibrations in the Type-II Superlattice InAs/InAs_{1-x}Sb_x

Henan Liu and Yong Zhang*

Optical Science and Engineering Graduate Program and Department of Electrical and Computer Engineering, University of North Carolina at Charlotte, Charlotte 28223, North Carolina, USA

Elizabeth H. Steenberg, Shi Liu, Zhiyuan Lin, and Yong-Hang Zhang

Center for Photonics Innovation and School of Electrical, Computer and Energy Engineering, Arizona State University, Tempe 85287, Arizona, USA

Jeomoh Kim, Mi-Hee Ji, Theeradetch Detchprohm, and Russell D. Dupuis

Center for Compound Semiconductors and School of Electrical and Computer Engineering, Georgia Institute of Technology, Atlanta 30332, Georgia, USA

Jin K. Kim, Samuel D. Hawkins, and John F. Klem

Sandia National Laboratories, Albuquerque 87185, New Mexico, USA

(Received 7 November 2016; revised manuscript received 9 August 2017; published 26 September 2017)

The InAs/InAs_{1-x}Sb_x superlattice system distinctly differs from two well-studied superlattice systems GaAs/AlAs and InAs/GaSb in terms of electronic band alignment, common elements at the interface, and phonon spectrum overlapping of the constituents. This fact leads to the unique electronic and vibrational properties of the InAs/InAs_{1-x}Sb_x system when compared to the other two systems. In this work, we report a polarized Raman study of the vibrational properties of the InAs/InAs_{1-x}Sb_x superlattices (SLs) as well as selected InAs_{1-x}Sb_x alloys, all grown on GaSb substrates by either MBE or metalorganic chemical vapor deposition (MOCVD) from both the growth surface and cleaved edge. In the SL, from the (001) backscattering geometry, an InAs-like longitudinal optical (LO) mode is observed as the primary feature, and its intensity is found to increase with increasing Sb composition. From the (110) cleaved-edge backscattering geometry, an InAs-like transverse optical (TO) mode is observed as the main feature in two cross-polarization configurations, but an additional InAs-like “forbidden” LO mode is observed in two parallel-polarization configurations. The InAs_{1-x}Sb_x alloys lattice matched to the substrate ($x_{\text{Sb}} \sim 0.09$) grown by MBE are also found to exhibit the forbidden LO mode, implying the existence of some unexpected [001] modulation. However, the strained samples ($x_{\text{Sb}} \sim 0.35$) grown by MOCVD are found to behave like a disordered alloy. The primary conclusions are (1) the InAs-like LO or TO mode can be either a confined or quasicontained mode in the InAs layers of the SL or extended mode of the whole structure depending on the Sb composition. (2) InAs/InAs_{1-x}Sb_x and InAs/GaSb SLs exhibit significantly different behaviors in the cleaved-edge geometry but qualitatively similar in the (001) geometry. (3) The appearance of the forbidden LO-like mode is a universal signature for SLs and bulk systems resulting from the mixing of phonon modes due to structural modulation or symmetry reduction.

DOI: 10.1103/PhysRevApplied.8.034028

I. INTRODUCTION

Recently, InAs/InAs_{1-x}Sb_x type-II superlattices (T2SLs) have received considerable attention as a new III-V-based infrared (IR) detection material [1,2], an alternative to the much more extensively studied InAs/GaSb T2SLs [3–6] that can complement the widely used bulk (Hg,Cd)Te alloys in mid- and long-wavelength infrared detection [7–10]. Improved minority-carrier lifetimes and dark currents compared to InAs/GaSb SLs have been reported for the InAs/InAs_{1-x}Sb_x SLs and their

devices [11,12], which are generally believed to be related to the absence of Ga in this system [13,14]. Therefore, this Ga-free system is becoming a research area in the fields of IR detection and basic material physics. In addition to the primary current interest in IR detection, the T2SLs offer the flexibility that type-I SLs, such as GaAs/AlAs SLs, do not have; that is, for the T2SLs, the electronic and thermal conductivity along the SL stacking direction can be tailored separately. This feature of the IR T2SL is highly desirable for thermoelectric related applications [15]. Additionally, if lateral contacts can be made separately from the two constituent layers to facilitate efficient carrier separation [16], IR T2SLs will be ideally suited for thermophotovoltaic devices [17].

*Corresponding author.
yong.zhang@unc.edu

In contrast to the considerable recent experimental efforts towards understanding the optical and electrical properties of InAs/InAs_{1-x}Sb_x SLs [1,11,18–22], there have not been many experimental or theoretical studies conducted on their vibrational properties or Raman spectroscopy, except for some early work on the InAs_{1-x}Sb_x alloys [23,24]. This situation motivates us to conduct a Raman study of the InAs/InAs_{1-x}Sb_x SLs, aiming to reveal and understand their vibrational properties and compare with two well-studied but distinctly different systems, GaAs/AlAs and InAs/GaSb SLs. This effort will fill the knowledge gap of our understanding of the Raman spectroscopy of semiconductor SLs because the InAs/InAs_{1-x}Sb_x system represents one of the three unique categories of SLs. This study lays the foundation for future efforts, such as exploring the mechanism of electron-phonon-coupling processes, using the results in material characterization, and providing guidance for device applications. Furthermore, this study provides the opportunity to uncover a fundamental and universal effect of structural modulation on longitudinal optical (LO) phonons in SLs and other modulated systems.

The InAs/InAs_{1-x}Sb_x system is unique when comparing its vibrational properties to those of the two better-known SL systems, GaAs/AlAs [25,26] and InAs/GaSb [27]. The GaAs/AlAs system has type-I or straddling electronic band alignment, and the optical phonon spectra of the two constituents do not overlap (resembling the so-called broken-gap type-II electronic band alignment but for the propagation band) [25]. InAs/GaSb has the broken-gap type-II electronic band alignment, and the optical phonon spectra of the two constituents overlap with each other but with one enclosing the other (resembling the type-I electronic band alignment) [28], whereas the InAs/InAs_{1-x}Sb_x system has staggered type-II electronic band alignment as well as staggered overlapping optical phonon spectra. Furthermore, InAs/GaSb is special, being a no-common-element system, whereas InAs/InAs_{1-x}Sb_x is a common-cation system. Consequently, the symmetry reduction from D_{2d} in the GaAs/AlAs to C_{2v} in the InAs/GaSb system does not occur in the InAs/InAs_{1-x}Sb_x system. Therefore, it is of great interest to investigate InAs/InAs_{1-x}Sb_x SLs, which will be beneficial for understanding the SL physics for this particular material system and the field in general.

One of the important SL effects related to symmetry reduction has been that the forbidden LO Raman mode in the (110) backscattering geometry in bulk becomes allowed, which was first observed in GaAs/AlAs SLs [29,30] and explained as arising from a standing wave in the SL stacking direction z with an effective large wave vector q_z [31]. Recently, the effect was observed in InAs/GaSb by some of us and speculated as due to the transverse mode of the phonon polariton [27]. The same effect was also observed in yet another system, a spontaneously ordered (Ga,In)P alloy—a monolayer superlattice

along the $[\bar{1}11]$ direction [32]. There were two possible mechanisms given: the q -dependent Fröhlich interaction and the Fröhlich interaction due to the electrical field induced by surface charges, in connection with the similar effect reported for a bulk material (GaAs) with doping [33]. We now add two cases, InAs/InAs_{1-x}Sb_x SLs and InAs_{1-x}Sb_x alloys, for this is fundamentally a symmetry-breaking-related phenomenon, which allows us to associate this phenomenon to a universal mechanism: modulation-induced mixing of vibration modes.

In this work, we perform polarized micro-Raman measurements on both a (001) growth plane and (110) cleaved edge on two sets of InAs/InAs_{1-x}Sb_x SL samples grown on GaSb substrates, one by molecular-beam epitaxy (MBE) and the other by metalorganic chemical vapor deposition (MOCVD), together with selected InAs_{1-x}Sb_x alloy samples, bulk InAs and InSb samples, and alloy and SL samples with Ga doping. The reasons to include a large set of samples are as follows: InAs_{1-x}Sb_x alloys are known to potentially exhibit both spontaneous vertical and lateral composition modulations, depending on the growth method and condition [34,35]. All the recent studies implicitly assumed the InAs_{1-x}Sb_x alloy layers in the SLs were disordered, even though samples were grown with different techniques. It is also well known that both lateral and vertical composition modulations in III-V alloys can have major effects in Raman scattering [32,36]. Our goal is to obtain the intrinsic properties of the SL assuming the alloy layer being disordered and alert the potential complications, if any, caused by any unintended structural modulation. Therefore, bulk alloys and SLs grown by different techniques are included. Furthermore, we show in our recent study of InAs/GaSb SLs that the relative Raman cross section of the bulk constituents can offer a very helpful hint to the origin of a Raman mode of the SL [27]. Thus, the bulk binaries are also measured under the same condition. Direct comparison of these samples is found to be important to understand the intrinsic vibrational properties of the SLs and reveal the subtle differences between the SL structures grown by the two growth techniques. Our primary findings include (1) an InAs (quasi-) confined LO mode when x_{Sb} is relatively low and its evolution into an extended SL mode when x_{Sb} increases observed from the front surface measurement; (2) an InAs (quasi-) confined transverse optical (TO) mode as well as a “forbidden” LO-like TO mode observed from the cleaved-edge measurement; (3) qualitatively different Raman spectra between InAs/InAs_{1-x}Sb_x and InAs/GaSb when measured from the (110) plane but qualitatively similar behaviors from the (001) plane; (4) the appearance of the LO-like mode in the forbidden geometry as a common feature in SLs and even bulk alloys when the translational symmetry is broken.

II. EXPERIMENT

All Raman measurements are conducted at room temperature using a Horiba HR800 confocal Raman microscope

TABLE I Sample information. *S* stands for superlattices; *A* stands for alloys. Labels in parentheses are original sample names.

Sample number	InAs/InAs _{1-x} Sb _x (nm)	Sb composition <i>x</i>	Total thickness (μm)	Notes
<i>S</i> _{MBE-1} (B1854)	7.7/2.4	0.205	2.5	100-nm InAs cap
<i>S</i> _{MBE-2} (B1871)	5.2/4.7	0.239	0.9	
<i>S</i> _{MBE-3} (B1775)	15.3/4.7	0.351	0.96	
<i>S</i> _{MBE-4} (B1816)	15.3/4.7	0.35	0.96	InAs _{1-x} Sb _x :Ga (center)
<i>S</i> _{MBE-5} (B1818)	15.3/4.7	0.35	0.96	InAs _{1-x} Sb _x :Ga (top and bottom)
<i>S</i> _{MOCVD-1} (3-2287)	13.3/5.59	0.255	0.57	
<i>S</i> _{MOCVD-2} (3-2289)	7.04/2.27	0.165	0.28	
<i>S</i> _{MOCVD-3} (3-2295)	5.29/4.80	0.230	1	
<i>S</i> _{MBE-6} (EB3610)	4.6/1.7	0.33	0.63	
<i>A</i> _{MBE-1} (B1784)	InAs _{1-x} Sb _x	0.09	1	
<i>A</i> _{MBE-2} (B1810)	InAs _{1-x} Sb _x	0.09	1	InAs _{1-x} Sb _x :Ga (top and bottom of the SL region)
<i>A</i> _{MBE-3} (B1814)	InAs _{1-x} Sb _x	0.09	1	InAs _{1-x} Sb _x :Ga [middle of the (In,As)Sb layers]
<i>A</i> _{MOCVD-1} (3-2483)	InAs _{1-x} Sb _x	0.343	0.3	75% relaxed
<i>A</i> _{MOCVD-2} (3-2489)	InAs _{1-x} Sb _x	0.355	0.5	79% relaxed
Bulk-1 (3-2296)	InAs			
Bulk-2 wafer	InSb			

equipped with a charge-coupled device. The Raman signals are collected by a 100 \times Olympus objective lens with numerical aperture NA = 0.9. The spectrometer is calibrated to yield the Si Raman peak at 520.7 cm⁻¹. By using a 532-nm laser, we have a spectral dispersion of 0.44 cm⁻¹/pixel and a spatial resolution of approximately 0.36 μm . To avoid sample heating, a sufficiently low laser power (approximately 0.22 mW) is used [27]. Typically, a redshift of approximately 1.5 cm⁻¹ is found for these samples when a factor of 10-times-higher laser power is used. Also, two additional Raman modes at approximately 131 cm⁻¹ and approximately 151 cm⁻¹ often appear at the higher power. We do not intend to discuss the details of the higher-power results, but we wish to point out that these features reported in the previous study of InAs_{1-x}Sb_x alloys [24] are actually from local heating-induced formation of Sb elemental crystal [37].

All samples are grown on (001) GaSb substrates either by MBE or MOCVD with their structural information listed in Table I. The samples are labeled with “*S*” for superlattice samples and “*A*” for alloy samples. Because the bulk lattice constant sizes are in the order of $a_{\text{InAs}}(6.0584 \text{ \AA}) < a_{\text{GaSb}}(6.0959 \text{ \AA}) < a_{\text{InSb}}(6.4794 \text{ \AA})$, InAs_{1-x}Sb_x is lattice matched to the GaSb substrate at $x_c = 0.089$. The SL structure overall is targeted to be lattice matched to the substrate, which means that the InAs layer will be under in-plane tensile strain and the InAs_{1-x}Sb_x layer under in-plane compressive strain if they are indeed coherently strained by the substrate. For $x > x_c$, the InAs_{1-x}Sb_x alloy is expected to be under in-plane compressive strain, if not relaxed. For MOCVD samples *S*_{MOCVD-1-3} and *A*_{MOCVD-1-2} (grown at Georgia Institute of Technology), the epilayers are grown in a close-coupled showerhead

MOCVD reactor system at 100 Torr on GaSb (100) \pm 0.04 $^\circ$ substrates. The carrier gas used is H₂ with the group-III precursors being trimethylindium and triethylgallium and the group-V precursors being trimethylantimony and arsine (AsH₃). The growth is carried out by first growing a 100-nm-thick GaSb buffer layer at 580 $^\circ\text{C}$, and then the temperature is ramped down to approximately 460 $^\circ\text{C}$ for the growth of the SL, InAs, or InAs_{1-x}Sb_x. For the MBE samples *S*_{MBE-1-5} and *A*_{MBE-1-3} (grown at Arizona State University), a GaSb buffer layer of 500 nm is grown at approximately 600 $^\circ\text{C}$, and then the temperature is ramped down to grow a 10-nm AlSb layer before growing the InAs_{1-x}Sb_x alloy layer or SL. The growth temperatures are in the range of 509–522 $^\circ\text{C}$ for the alloy samples and 420–464 $^\circ\text{C}$ for the SL samples. These samples are all capped with 10-nm AlSb followed by 10-nm GaSb, except for *S*_{MBE-1} that is capped by 100-nm InAs. MBE sample *S*_{MBE-6} (grown at Sandia National Laboratories) is grown at approximately 420 $^\circ\text{C}$. More growth details can be found in Refs. [38–40]. The compositions of the InAs_{1-x}Sb_x alloys and InAs_{1-x}Sb_x alloy layers in the SLs are determined by x-ray analyses. The individual layers in the SL samples are found to be nearly coherently strained by the substrate [39], and the two relatively high Sb composition alloy samples are found to be partially relaxed (*A*_{MOCVD-1}, approximately 75%; *A*_{MOCVD-2}, approximately 79%). The details of the x-ray analysis methods can be found in our previous publications [38,39]. We note that the compositions are derived under the assumption of an abrupt Sb profile. Although the actual Sb profile has been found to be more complex [40], the relative order of the compositions should remain correct among the SL samples if grown by the same technique. Therefore, the general understanding and conclusions on the

SLs to be given in this work are not affected by the precise value of the alloy composition and profile.

III. RESULTS AND DISCUSSION

A. InAs_{1-x}Sb_x alloys

We first compare the Raman spectra of bulk InAs and InSb, as shown in Fig. 1, with Fig. 1(a) for (001) backscattering and Fig. 1(b) for (110) backscattering. These two geometries yield, respectively, the LO and TO phonon modes at 238.5 and 217.4 cm⁻¹ for InAs and 190.0 and 179.6 cm⁻¹ for InSb. For both geometries, the Raman cross sections of InSb are approximately a factor of 2 larger than those of InAs.

Figure 2 shows (001) backscattering Raman spectra for two InAs_{1-x}Sb_x alloy samples: $A_{\text{MBE-1}}$ with $x_{\text{Sb}} = 0.09$ in Fig. 2(a) and $A_{\text{MOCVD-2}}$ with $x_{\text{Sb}} = 0.355$ in Fig. 2(b) under four polarization configurations: $z(x',x')\bar{z}$, $z(y',y')\bar{z}$, $z(x',y')\bar{z}$, and $z(y',x')\bar{z}$. Here, we adopt the conventions that x' , y' , and z' are defined as $x' \sim [110]$, $y' \sim [\bar{1}10]$, and $z' \sim [001]$, with respect to the cubic axes $x \sim [100]$, $y \sim [010]$, and $z \sim [001]$. If the alloy is viewed as having T_d symmetry on average, the two parallel-polarization configurations are equivalent and both are allowed for the LO-like phonons, and two cross-polarization configurations are forbidden. Indeed, the alloy samples seem to obey the selection rules (Table II) for T_d symmetry in this scattering geometry. The primary peak in both alloy samples should be the InAs-like LO mode (LO1), although for the higher- x_{Sb} samples, an InSb-like LO mode (LO2) is also observed, as reported previously for InAs_{1-x}Sb_x alloys [24]. However, $A_{\text{MBE-1}}$ exhibits a small anisotropy in intensity (approximately 20%) between $[110]$ and $[\bar{1}10]$, indicating lower symmetry than T_d .

Figure 3 shows the comparison between the Raman frequencies of the LO1 mode from our alloy samples and the composition dependence of the LO1 mode for

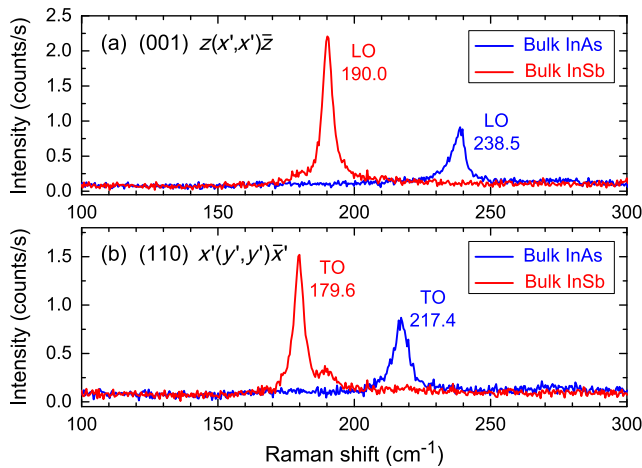


FIG. 1 Raman spectra of bulk InAs and InSb. (a) (001) backscattering, (b) (110) backscattering.

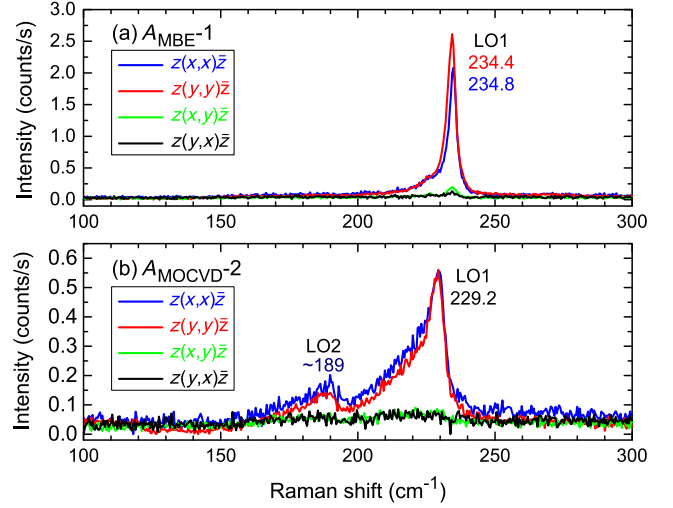


FIG. 2 (001) backscattering Raman spectra of InAs_{1-x}Sb_x alloys in four polarization configurations. (a) $A_{\text{MBE-1}}$ ($x_{\text{Sb}} = 0.09$), (b) $A_{\text{MOCVD-2}}$ ($x_{\text{Sb}} = 0.355$).

fully relaxed alloys given in the previous report [24]: $\text{LO1}(\text{cm}^{-1}) = 238.5 - 32 x_{\text{Sb}}$ (replacing the $x_{\text{Sb}} = 0$ value with the current room-temperature value). Apparently, the observed LO1 frequency of approximately 229 cm⁻¹ for the $x_{\text{Sb}} = 0.355$ sample lies above the curve for fully relaxed alloys but significantly lower than the predicted curve for alloys under coherency strain with the substrate (the calculation is described later). The comparison indicates that the epitaxial layers are partially relaxed, which is consistent with the XRD analysis, suggesting that samples $A_{\text{MOCVD-1}}$ and $A_{\text{MOCVD-2}}$ are, respectively, 75% and 79% relaxed.

The (110) backscattering spectra are shown in Fig. 4 in four polarization configurations for the same two alloy samples used in Fig. 2. In T_d symmetry, the TO mode is forbidden in (001) backscattering but allowed in (110) backscattering [41]. However, in the previous report, the (In,As)Sb TO modes were actually measured from (001) backscattering due to the relaxation of the symmetry selection rule in an alloy but only in a range of $x_{\text{Sb}} \leq 0.23$ [24]. Now, we are able to examine the TO modes directly in (110) backscattering. For T_d symmetry, the three configurations $x'(y',z)\bar{x}'$, $x'(z,y')\bar{x}'$, and $x'(y',y')\bar{x}'$ are allowed and equivalent, and $x'(z,z)\bar{x}'$ is forbidden (see Table II) [41]. We note that despite the three allowed configurations being equivalent in T_d , $x'(y',z)\bar{x}'$ and $x'(z,y')\bar{x}'$ are associated with the vibrations in the x - y plane, while $x'(y',y')\bar{x}'$ is associated with the vibrations along the z direction. Therefore, any modulation along the z direction, for instance, in a SL, will make $x'(y',y')\bar{x}'$ different from the other two. For the alloy sample, the three configurations should remain equivalent in the ideal situation. For the alloy sample $A_{\text{MBE-1}}$ with $x_{\text{Sb}} = 0.09$, as shown in Fig. 4(a), the $x'(y',z)\bar{x}'$ and $x'(z,y')\bar{x}'$

TABLE II Raman selection rules for D_{2d} and T_d Raman modes in (001) and (110) backscattering geometries. The notations x, y, x', y' , and z refer to $x \sim [100]$, $y \sim [010]$, $x' \sim [110]$, $y' \sim [\bar{1}10]$, and $z \sim [001]$, respectively.

Symmetry group	D_{2d}				T_d		
	Symmetry						
Geometry	$E(x)$	$E(y)$	$B_2(z)$	A_1	$F_2(x)$	$F_2(y)$	$F_2(z)$
$z(x', x')\bar{z}$	0	0	d_{LO}^2	a_{LO}^2	0	0	d_{LO}^2
$z(y', y')\bar{z}$	0	0	d_{LO}^2	a_{LO}^2	0	0	d_{LO}^2
$z(x', y')\bar{z}$	0	0	0	0	0	0	0
$z(y', x')\bar{z}$	0	0	0	0	0	0	0
$x'(y', y')\bar{x}'$	0	0	d_{TO}^2	a_{TO}^2	0	0	d_{TO}^2
$x'(z, z)\bar{x}'$	0	0	0	b_{TO}^2	0	0	0
$x'(y', z)\bar{x}'$	$e_{TO}^2/2$	$e_{TO}^2/2$	0	0	$d_{TO}^2/2$	$d_{TO}^2/2$	0
$x'(z, y')\bar{x}'$	$e_{TO}^2/2$	$e_{TO}^2/2$	0	0	$d_{TO}^2/2$	$d_{TO}^2/2$	0

configurations are indeed very similar as expected. The primary Raman mode at approximately 215.5 cm^{-1} should be the InAs-like TO mode (TO1) of the $\text{InAs}_{1-x}\text{Sb}_x$ alloy [24]. The weak peak at approximately 226 cm^{-1} is the TO

mode of the GaSb substrate because the epilayer is relatively thin compared to the laser spot size. However, interestingly, the $x'(y', y')\bar{x}'$ configuration in Fig. 4(b) turns out to be very different from the other two, and the $x'(z, z)\bar{x}'$ configuration is also not as weak as one expects. More peculiar is the appearance of a Raman mode at approximately 234.5 cm^{-1} , close to the LO1 mode that is observed in (001) backscattering. Thus, although this sample is supposed to be an alloy, it behaves more like a superlattice with some sort of modulation along the [001] direction. We note that the same peak is also observed in the two Ga-doped samples ($A_{\text{MBE}-2}$ and $A_{\text{MBE}-3}$) but weaker relative to TO1. We come back to discuss the origin of this mode later when presenting the similar phenomenon observed in the SLs.

For the alloy sample $A_{\text{MOCVD}-2}$ with $x_{\text{Sb}} = 0.355$, as shown in Figs. 4(c) and 4(d), in contrast to the lower- x_{Sb} sample $A_{\text{MBE}-1}$, this sample behaves more like a bulk material of T_d symmetry, and interestingly, the LO1 peak is absent. The Raman mode at approximately 211 cm^{-1} can be assigned as TO1 and the other one at approximately 187 cm^{-1} can be the InSb-like TO mode (TO2) of the alloy, which was not found previously [24]. The TO1 mode frequencies for the alloys are plotted in Fig. 3(b) comparing to the composition dependence of Ref. [24]: $\text{TO1}(\text{cm}^{-1}) = 217.4 - 27 x_{\text{Sb}}$ for $x_{\text{Sb}} \leq 0.23$ (replacing the $x_{\text{Sb}} = 0$ value with the current room-temperature value). The contrast between the two samples does not appear to be incidental because the three lower- x_{Sb} samples (see Table I) behave qualitatively the same (more discussions are given later), and the two high- x_{Sb} samples are also found to be similar. However, we cannot simply attribute the difference to the composition dependence because one set of samples is grown by MBE, while the other by MOCVD. It is well known that different types of composition modulations may occur in III-V alloys, and the specific form of the modulation depends sensitively on the growth method and condition [42]. Therefore, more systematic investigation is required to understand the microscopic structures of the alloys.

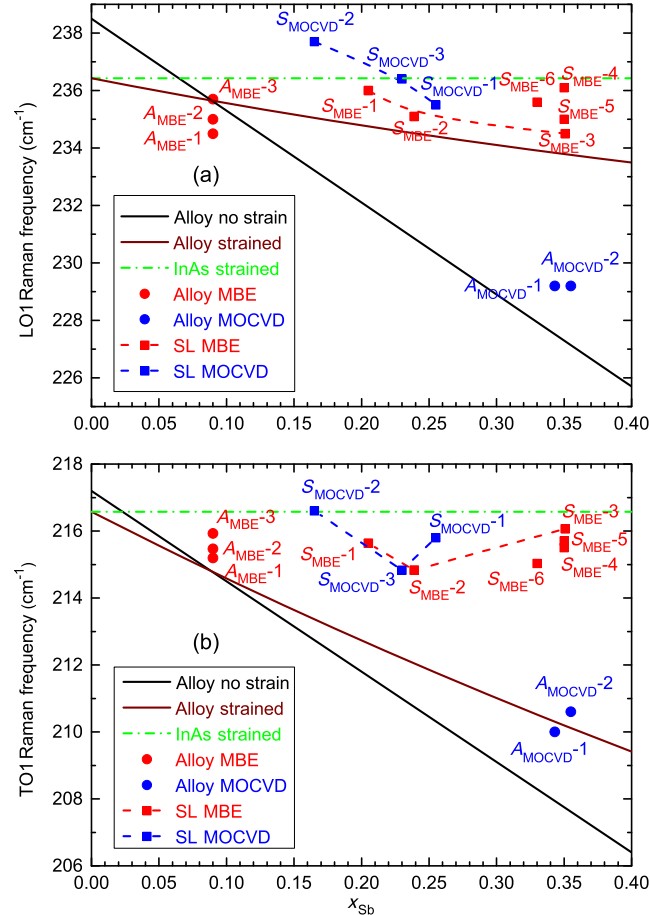


FIG. 3 Sb composition dependence of phonon frequency: (a) for the InAs-like LO phonon, (b) for the InAs-like TO phonon calculated for alloys with and without strain (solid lines) and for strained InAs (dashed lines), and measured (symbols) for alloys (circular points) and superlattices (square points).

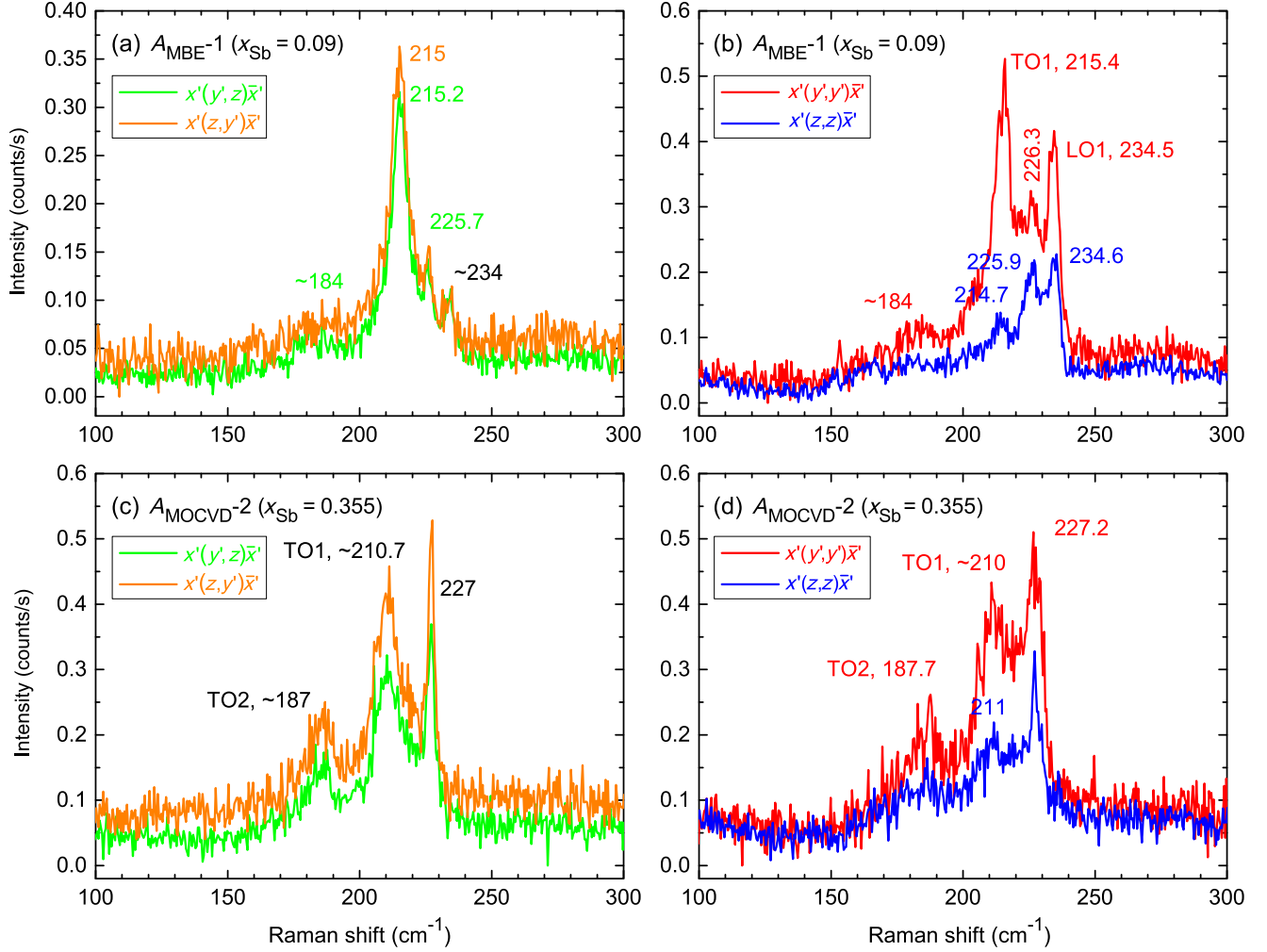


FIG. 4 (110) backscattering Raman spectra of $\text{InAs}_{1-x}\text{Sb}_x$ alloys in four polarization configurations for the same samples of Fig. 2. (a) $A_{\text{MBE-1}}$ ($x_{\text{Sb}} = 0.09$), (b) $A_{\text{MOCVD-2}}$ ($x_{\text{Sb}} = 0.355$).

B. $\text{InAs}/\text{InAs}_{1-x}\text{Sb}_x$ superlattices

Figure 5 compares the spectra of the four polarization configurations for two SL samples with very similar structures, $S_{\text{MOCVD-3}}$ ($x_{\text{Sb}} = 0.230$) in Figs. 5(a) and 5(b) and $S_{\text{MBE-2}}$ ($x_{\text{Sb}} = 0.239$) in Figs. 5(c) and 5(d) grown, respectively, by MOCVD and MBE. The former exhibits $\text{LO1} = 236.4 \text{ cm}^{-1}$ and the latter $\text{LO1} = 235.1 \text{ cm}^{-1}$. Their frequencies are substantially higher than that expected for the corresponding free-standing $\text{InAs}_{1-x}\text{Sb}_x$ alloy at the same composition of approximately 230.8 cm^{-1} but matching or close to the expected values for InAs under tensile strain of approximately 236.4 cm^{-1} or $\text{InAs}_{1-x}\text{Sb}_x$ alloy under compressive strain of approximately 234.5 cm^{-1} . The strain effects can be calculated using these formulas from the literature, for instance, Ref. [43]:

$$\delta\omega_{\text{LO}} = \delta\omega_{\text{H}} + 2/3\delta\omega_{\text{S}}, \quad (1)$$

$$\delta\omega_{\text{TO}} = \delta\omega_{\text{H}} - 1/3\delta\omega_{\text{S}} \quad (2)$$

with

$$\delta\omega_{\text{H}} = -\omega_0\gamma(\epsilon_{xx} + \epsilon_{yy} + \epsilon_{zz}), \quad (3)$$

$$\delta\omega_{\text{S}} = -\omega_0\lambda(\epsilon_{xx} - \epsilon_{zz}), \quad (4)$$

where $\delta\omega_{\text{H}}$ and $\delta\omega_{\text{S}}$ are, respectively, the contributions of hydrostatic and biaxial or uniaxial strain, $\gamma = -(p + 2q)/(6\omega_0^2)$ and $\lambda = (p - q)/(2\omega_0^2)$ are the corresponding dimensionless deformation potentials, the strain tensor components are $\epsilon_{xx} = \epsilon_{yy} = (a_{\text{GaSb}} - a_{(\text{In,As})\text{Sb}})/a_{(\text{In,As})\text{Sb}}$, $\epsilon_{zz} = -2C_{12}/C_{11}\epsilon_{xx}$, C_{12} and C_{11} are elastic constants, and ω_0 is the corresponding alloy phonon frequency at zero strain. The values for all the parameters are obtained by linear interpolation between InAs and InSb , except for the composition dependence of the phonon frequency taken from Ref. [24]. The LO1 values for all the SL samples are plotted in Fig. 3(a), in comparison with three calculated curves: the strain-free $\text{InAs}_{1-x}\text{Sb}_x$ (black), strained $\text{InAs}_{1-x}\text{Sb}_x$ (wine),

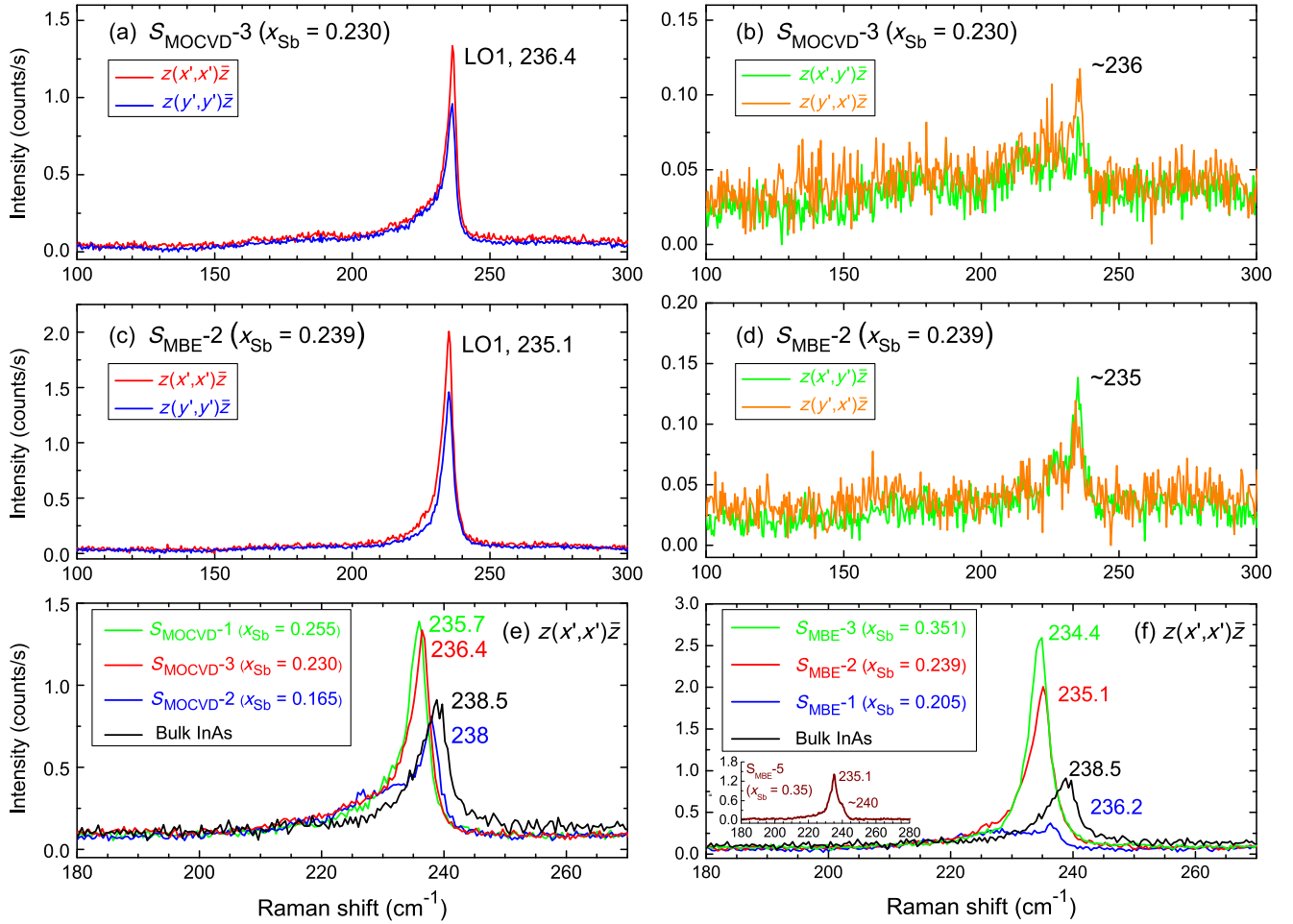


FIG. 5 (001) backscattering Raman spectra of $\text{InAs}/\text{InAs}_{1-x}\text{Sb}_x$ superlattices. (a)–(d) For two samples with similar structural parameters grown, respectively, by MOCVD and MBE, in four polarization configurations. (e), (f), respectively, compare different superlattice samples grown by MOCVD and MBE with bulk InAs. The inset of (f) shows an additional MBE sample with Ga doping.

and strained InAs (green) under the coherency epitaxial strain. Apparently, the LO1 frequencies of SLs mostly fall between the last two curves. Similar to the situation in InAs/GaSb SLs [44,45], there are three possible mechanisms for the LO1 mode: (1) InAs confined mode, (2) InAs quasiconfined mode, and (3) extended mode. There is yet another possibility; that is, the LO1 is simply the LO mode (mostly) from the strained $\text{InAs}_{1-x}\text{Sb}_x$ layers, namely, an $\text{InAs}_{1-x}\text{Sb}_x$ (quasi-) confined mode similar to the case of $\text{Ge}_x\text{Si}_{1-x}/\text{Si}$ SLs grown on Si substrates where the Raman modes were suggested to be originated from the strained alloy layer [46]. By examining the relative intensity of the LO1 mode in the two sets of SL samples with respect to bulk InAs, as shown in Fig. 5(e) for $S_{\text{MOCVD-2}}$, $S_{\text{MOCVD-3}}$, $S_{\text{MOCVD-1}}$, and Fig. 5(f) for $S_{\text{MBE-1}}$, $S_{\text{MBE-2}}$, and $S_{\text{MBE-3}}$, as well as the LO1 frequencies in Fig. 3(a), we find that with increasing x_{Sb} from $x_{\text{Sb}} \sim 0.165$ to $x_{\text{Sb}} \sim 0.35$, the LO1 intensity increases significantly (exceeding that in bulk InAs), while the frequency redshifts from that of strain-free InAs (approximately 238.5 cm^{-1}) or strained InAs

(approximately 236.4 cm^{-1}) but remains above that of strained $\text{InAs}_{1-x}\text{Sb}_x$ of the same x_{Sb} . The particularly weak signal for $S_{\text{MBE-1}}$ in Fig. 5(f) can be partially due to the presence of the 100-nm InAs capping layer. If the Raman signal is from the $\text{InAs}_{1-x}\text{Sb}_x$ layer, as the first-order approximation that the Raman signal is proportional to the fraction of the alloy layer in the superlattice period, the signal intensity will be much below that of the bulk InAs, which is apparently contradicting the experimental results. These trends suggest that LO1 is likely an InAs confined or quasiconfined mode in the InAs layers when x_{Sb} is relatively low (e.g., near 0.16) and becomes an extended SL mode for the higher x_{Sb} values. In the higher- x_{Sb} region, the InAs confined or quasiconfined mode might continue to exist but cannot be resolved due to the smaller Raman cross section of InAs and perhaps other effects such as structural imperfection. The situation is similar to the case of InAs/GaSb where the theoretically predicted InAs confined or quasiconfined modes are not observable [27]. It is worth mentioning that in one Ga-doped sample ($S_{\text{MBE-5}}$) with $x_{\text{Sb}} = 0.35$, an

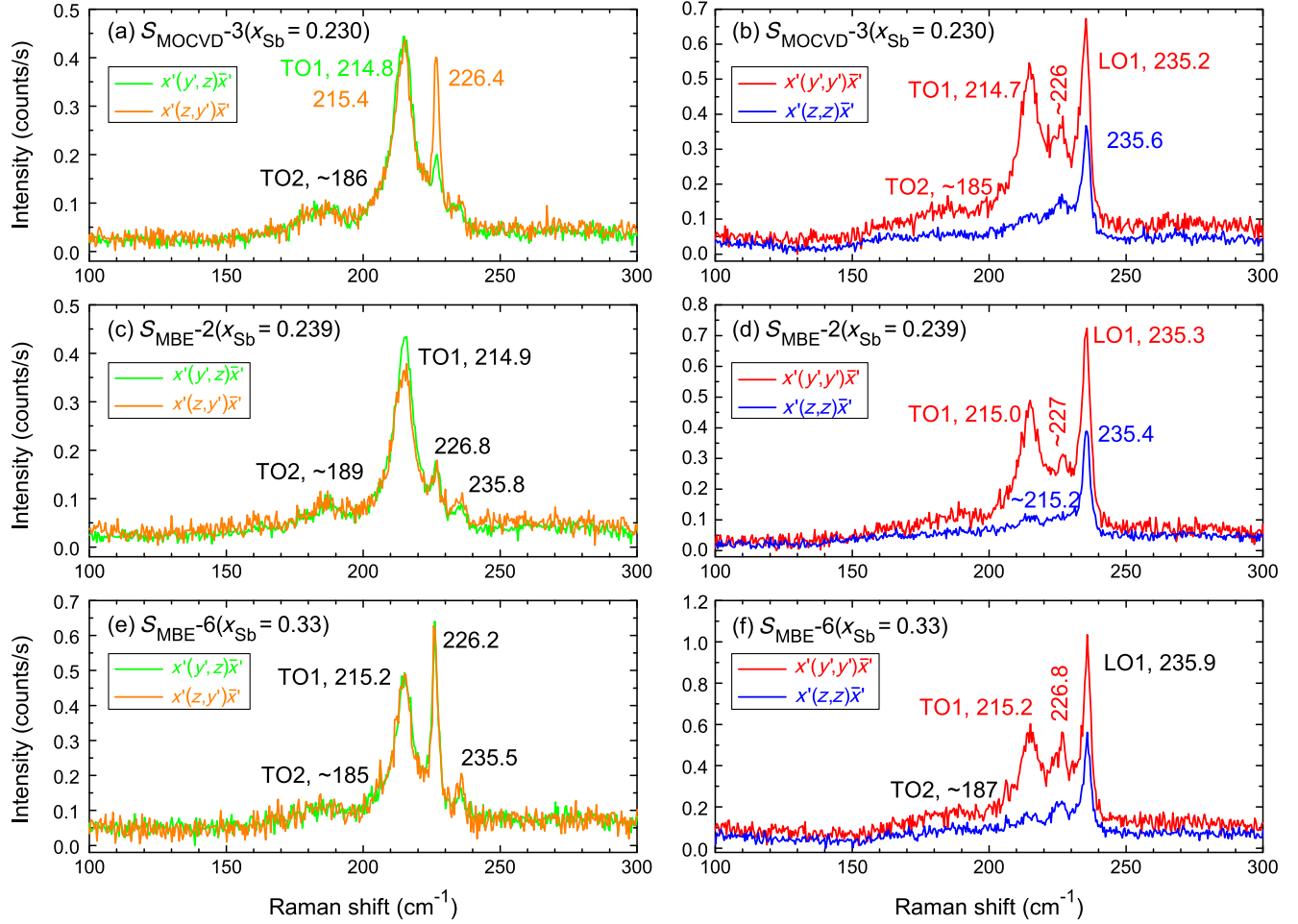


FIG. 6 (110) backscattering Raman spectra of InAs/InAs_{1-x}Sb_x superlattices. (a)–(d) For two samples with similar structural parameters grown, respectively, by MOCVD and MBE, in four polarization configurations. (e),(f) For another MBE sample grown by a different growth system.

additional weaker Raman mode at approximately 240 cm⁻¹, close to that of InAs (approximately 238.5 cm⁻¹), is observed on the higher-frequency side of the main peak, as shown in the inset of Fig. 5(f). Confined or quasicontained modes in the InAs_{1-x}Sb_x layers are unlikely to occur unless in a very high x_{Sb} value [44,45], which means that the observed superlattice LO1 mode cannot be the pure InAs_{1-x}Sb_x alloy mode that would be given by the strained InAs_{1-x}Sb_x curve in Fig. 3(a). This understanding is expected to be relevant to the somewhat similar system Ge_xSi_{1-x}/Si SL [47].

The polarization dependence of the (001) scattering shown in Fig. 5 indicates that the InAs/InAs_{1-x}Sb_x SL obeys the Raman selection rules (see Table II) for the SL with D_{2d} symmetry with these four allowed Raman tensors given in the basis of (x, y, z) as $A_1 = [(a, 0, 0), (0, a, 0), (0, 0, b)]$, $B_2(z) = [(0, d, 0), (d, 0, 0), (0, 0, 0)]$, $E(x) = [(0, 0, 0), (0, 0, e), (0, e, 0)]$, and $E(y) = [(0, 0, e), (0, 0, 0), (e, 0, 0)]$ [29,48]. In general, the (001) backscattering spectra of the InAs/InAs_{1-x}Sb_x SLs are

rather similar to those of InAs/GaSb [27]. Namely, they primarily show one major peak with broadening toward the lower-frequency side, obeying the similar Raman selection rules as in the bulk. Therefore, they do not offer as much information about the vibrational properties of the SL as the spectra from the (110) cleaved edge [27].

We now examine the cleaved-edge results. Figure 6 shows the (110) backscattering spectra of three SL samples in four polarization configurations for the same two samples ($x_{\text{Sb}} = 0.230, 0.239$) used in Figs. 5(a) and 5(b) and another one with a higher composition $x_{\text{Sb}} = 0.33$ ($S_{\text{MBE}}-6$) and also from a different source. The polarization dependence is found to be qualitatively similar to the MBE alloy sample with $x = 0.09$ shown in Fig. 4(a). The two cross-polarization configurations $x'(y',z)\bar{x}'$ and $x'(z,y')\bar{x}'$ are related to the TO modes that vibrate in the x - y plane described by the Raman tensor $E(x)$ or $E(y)$. The primary Raman peak is the InAs-like TO mode referred to as TO1 and the much weaker peak is the InSb-like TO mode (TO2). The TO1 mode frequencies for all SLs are summarized in

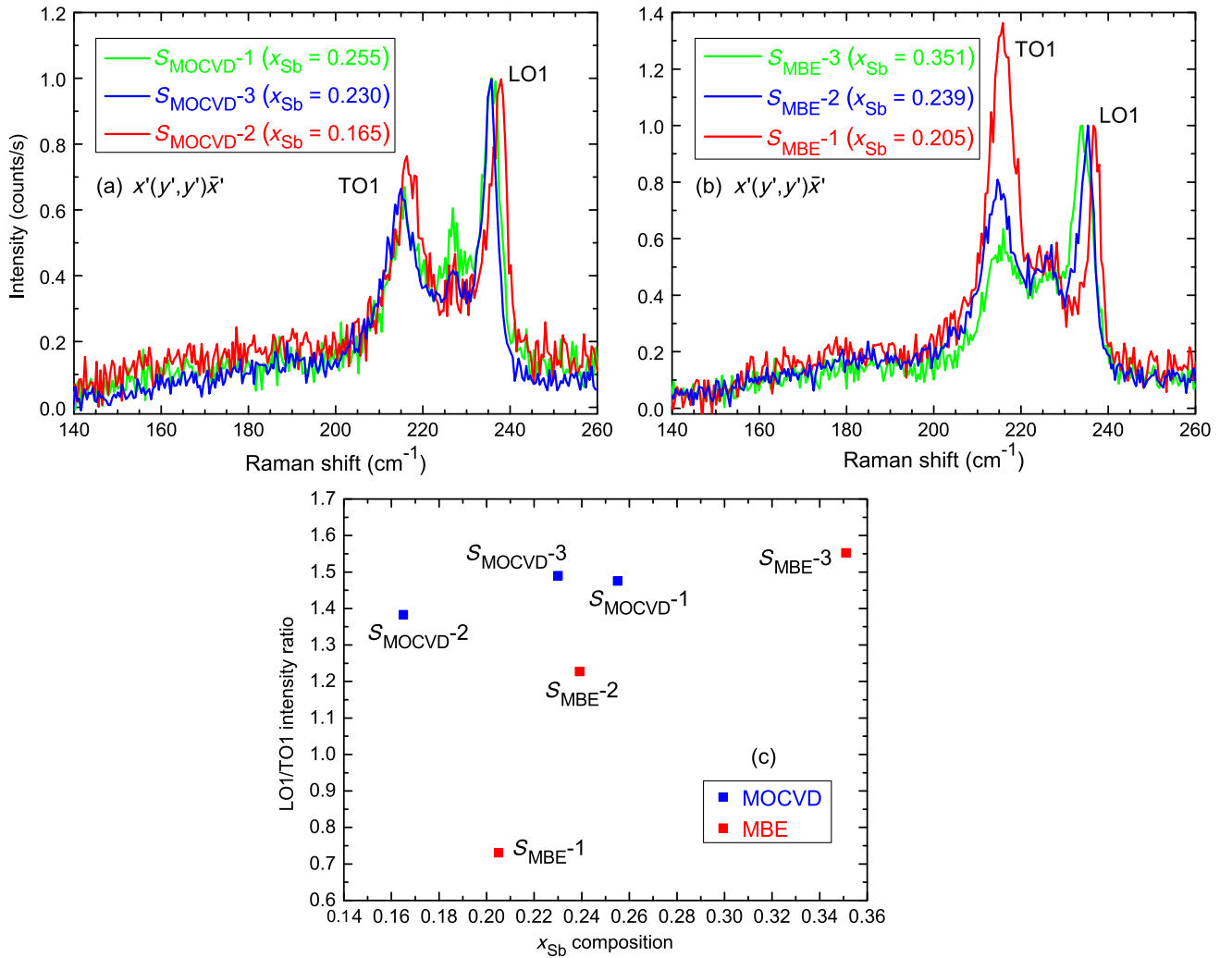


FIG. 7 Sb composition dependence of the forbidden LO-like mode in InAs/InAs_{1-x}Sb_x superlattices observed in the (110) backscattering geometry. The spectra are normalized to the LO-like mode. (a),(b), respectively, for MOCVD and MBE samples. (c) The peak intensity ratio of the LO-like mode to TO mode.

Fig. 3(b), compared with the values for the strain-free InAs_{1-x}Sb_x, strained InAs_{1-x}Sb_x, and strained InAs. The intensities of the TO1 mode are found to be comparable to but weaker than that of the bulk InAs. However, the intensity comparison is less reliable for the cleaved-edge measurement because of the overall small thickness of the SL region. The frequencies of the TO1 modes are substantially higher than the corresponding values of the strained InAs_{1-x}Sb_x alloys. Thus, this mode is unlikely originated from the strained alloy layers. For the relatively low- x_{Sb} sample (e.g., $x_{\text{Sb}} \sim 0.16$), the TO1 frequency is very close to that of strained InAs; thus, TO1 is likely a confined or quasicontained TO mode in the InAs layers. For the higher- x_{Sb} samples, the TO1 frequencies fall between the two limits, as shown in Fig. 3(b); thus, it is reasonable to assume they are extended modes of the SL as a whole. These assignments are similar to the LO1 mode obtained from the (001) backscattering.

In the two parallel configurations, $x'(y',y')\bar{x}'$ and $x'(z,z)\bar{x}'$, a peak close to the LO1 frequency is observed. For the (001) SL, both A_1 and $B_2(z)$ modes with vibration along z are allowed for $x'(y',y')\bar{x}'$, and only the A_1 mode is allowed for $x'(z,z)\bar{x}'$ (see Table II) [29]. $B_2(z)$ is originated from the deformation potential and A_1 from the Fröhlich interaction, which qualitatively explains the intensity difference between the two configurations [29]. In fact, including the earlier observations in GaAs/AlAs [29], the spontaneously ordered (Ga,In)P alloy [32], and the recent finding in the InAs/GaSb SLs [27], the appearance of a LO mode in the forbidden geometry has now been established as a common feature of the SL structures. A simple explanation of the LO1-like mode in this geometry is that the phonon mode with a small wave vector along x' (to satisfy the momentum conservation) has a standing wave motion along the z direction (with $q_z = 0$) due to zone folding in the SL; thus, the participating phonon mode has a large

effective wave vector in the z direction [31]. Technically, this is a TO mode with a small SL wave vector along x' to satisfy the momentum conservation but with large q_z components of the bulk phonon modes, whereas the (001) scattering involves a LO mode with a small SL wave vector along z but, nevertheless, may have large q_z components of the folded bulk phonon modes. Therefore, the LO modes observed in the two scattering configurations can involve the similar components of the folded bulk phonon modes but with different SL wave vectors, respectively, along the z and x' directions, and, thus, their frequencies are slightly different and can be viewed as the longitudinal and transverse modes of the phonon polariton in the SL.

Figure 7 compares the spectra of the $x'(y', y')\bar{x}'$ configuration normalized to LO1 for two sets of samples, $S_{\text{MOCVD-2}}$, $S_{\text{MOCVD-3}}$, $S_{\text{MOCVD-1}}$ and $S_{\text{MBE-1}}$, $S_{\text{MBE-2}}$, $S_{\text{MBE-3}}$, respectively, in Figs. 7(a) and 7(b), with their peak intensity ratios between LO1 and TO1 plotted in Fig. 7(c). Interestingly, we find that the intensity ratio of the LO1 mode to the TO1 mode increases with increasing the Sb composition of the $\text{InAs}_{1-x}\text{Sb}_x$ layer, which can be understood as due to enhanced modulation in elastic and electronic properties with increasing contrast between the InAs and $\text{InAs}_{1-x}\text{Sb}_x$ layer. It appears that this intensity ratio can serve as an empirical measure of the deviation from the bulk as a result of vertical structural modulation. With this understanding, we may speculate that the results observed for the alloy sample with $x_{\text{Sb}} = 0.09$ suggest the possible existence of unintended vertical modulation. Although such modulation might not be periodic as in a SL (thus, no standing wave formation), the perturbation seems to be sufficient to induce some phonon-scattering effects that may also lead to the mixture of the modes with different q_z values. Spontaneous composition modulation along the z axis has been reported in $\text{InAs}_{1-x}\text{Sb}_x$ alloys with $0.4 \leq x_{\text{Sb}} \leq 0.8$ [35], although not in such a low composition. More careful structural study is required to identify the exact nature of the modulation, but cleaved-edge-polarized Raman spectroscopy shows to be a very sensitive tool for revealing the existence of the modulation.

IV. COMPARISON BETWEEN $\text{InAs}/\text{InAs}_{1-x}\text{Sb}_x$, InAs/GaSb , AND GaAs/AlAs SUPERLATTICES

In the (001) backscattering geometry, the selection rules in the SLs for the four commonly adopted configurations $z(x', x')\bar{z}$, $z(y', y')\bar{z}$, $z(x', y')\bar{z}$, and $z(y', x')\bar{z}$ are usually the same as in the bulk. It is rather unique that for GaAs/AlAs SLs, multiple confined LO modes can be observed, benefiting from their LO phonon spectra being well separated [49]. For both InAs/GaSb SLs [27] and $\text{InAs}/\text{InAs}_{1-x}\text{Sb}_x$ SLs (Fig. 5), there is only one primary LO mode. Therefore, the Raman scattering results of this geometry are not very informative for understanding the

vibrational properties of the SLs, and no qualitatively difference is revealed between the two systems.

It is the (110) backscattering geometry that reveals some interesting and subtle differences between these two systems. To show clearly the similarity and difference, in Fig. 8 we compare the typical spectra of the two systems (using sample $S_{\text{MBE-2}}$ and sample IFA in Ref. [27]) measured under comparable conditions in four important configurations. For $z(x', x')\bar{z}$ of the (001) backscattering, Fig. 8(a) shows only one primary LO mode for each SL. However, there are some interesting differences: for the $\text{InAs}/\text{InAs}_{1-x}\text{Sb}_x$ SL, there is an extended InAs-like LO mode (LO1) that is stronger than that of bulk InAs [Fig. 5(f)]; for the InAs/GaSb SL, there is a quasicontained GaSb-like LO mode that is weaker than that of the bulk GaSb, with a further weaker GaSb-like TO mode but no expected confined InAs LO mode [27]. For the (110) backscattering, the two cross-polarization configurations $x'(y', z)\bar{x}'$ and $x'(z, y')\bar{x}'$ are always very similar for all above-mentioned SLs ([27,29,30] and Fig. 6), as dictated by the symmetry and associated with the TO mode with vibration along y . Thus, Figs. 8(b)–8(d) compare the three configurations of the (110) backscattering between the two systems: $x'(y', z)\bar{x}'$, $x'(y', y')\bar{x}'$, and $x'(z, z)\bar{x}'$. For $x'(y', z)\bar{x}'$ of Fig. 8(b), the InAs/GaSb SL exhibits a GaSb confined TO mode, an InAs-like quasicontained TO mode, and a weak InSb-like interface mode, whereas the $\text{InAs}/\text{InAs}_{1-x}\text{Sb}_x$ SL shows an extended InAs-like TO1 mode and a weak, confined InSb-like TO2 mode. For $x'(y', y')\bar{x}'$ of Fig. 8(c), the InAs/GaSb SL exhibits a rather different spectrum from the cross polarization, namely, with primarily an extended TO mode, whereas the $\text{InAs}/\text{InAs}_{1-x}\text{Sb}_x$ SL yields the same TO features as in the cross polarization, similar to the case of GaAs/AlAs SLs [29,30]. And for all the three SL systems, a forbidden LO-like mode appears in this configuration. Furthermore, for $x'(z, z)\bar{x}'$ of Fig. 8(d), which is a forbidden configuration under T_d symmetry but allowed for the SL A_1 mode, the LO-like mode as well as other modes are usually very weak compared to $x'(y', y')\bar{x}'$, as in the cases for the InAs/GaSb SL and GaAs/AlAs SLs [27,29]. However, for the $\text{InAs}/\text{InAs}_{1-x}\text{Sb}_x$ SL, the intensity of the LO-like mode is about one-half of that in $x'(y', y')\bar{x}'$. It turns out that the situation in the $\text{InAs}/\text{InAs}_{1-x}\text{Sb}_x$ SLs is actually very similar to that of spontaneously ordered (Ga,In)P alloy on the cleaved edge [32].

V. SUMMARY AND CONCLUSIONS

In summary, we observe several intrinsic vibrational features in $\text{InAs}/\text{InAs}_{1-x}\text{Sb}_x$ SLs. In the (001) backscattering geometry, a confined or quasicontained InAs LO mode (LO1 mode) is revealed when x_{Sb} is near 0.16, which then evolves into an extended SL mode for higher x_{Sb} values. In the (110) backscattering geometry, two modes are revealed: an InAs-like TO mode (TO1) with $E(x)$ or $E(y)$ symmetry

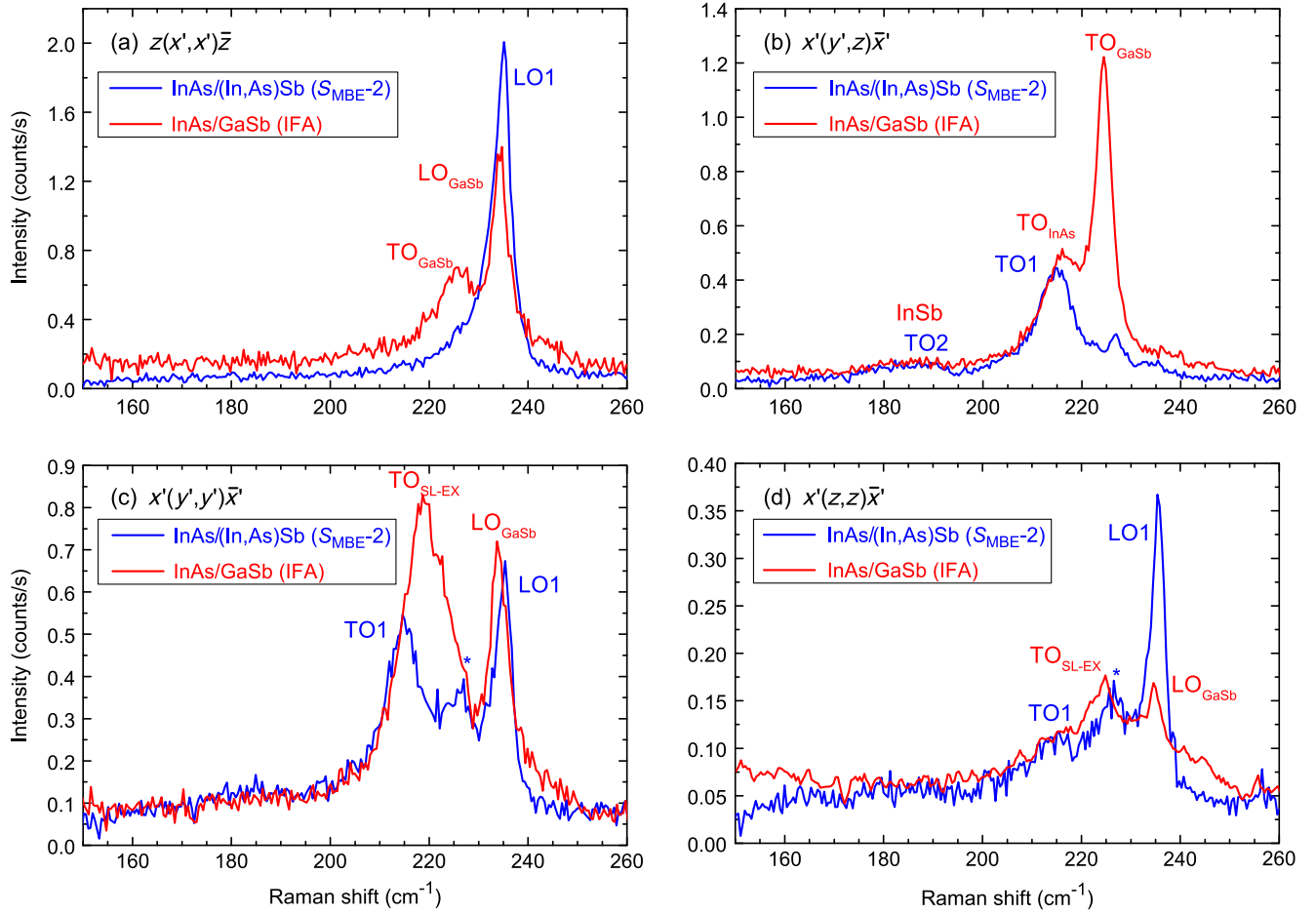


FIG. 8 Comparison between InAs/InAs_{1-x}Sb_x and InAs/GaSb superlattices: (a) for (001) backscattering, (b)–(d) for (110) backscattering in three polarization configurations. The peak indicated by “star” is from the GaSb substrate in the spectra for the InAs/InAs_{1-x}Sb_x superlattice.

that also evolves from an InAs confined or quasicontained mode into an extended mode with increasing x_{Sb} and a LO1-like mode with A_1 and $B_2(z)$ symmetry.

The InAs_{1-x}Sb_x alloys grown by MBE with x_{Sb} lattice matching to the GaSb substrate are found to possibly have some structural modulation along the growth direction. Additionally, Ga-doping effects are also briefly examined for InAs/InAs_{1-x}Sb_x SLs and InAs_{1-x}Sb_x alloys. Two previously reported unexplained peaks in InAs_{1-x}Sb_x alloys are found to be the result of unintended laser-induced formation of Sb elemental crystal.

A LO-like mode has now been established as a common feature observable in the backscattering geometry from the plane containing the axis of the structural modulation, for instance, the (110) plane for a [001] superlattice as in GaAs/AlAs, InAs/GaSb, and InAs/InAs_{1-x}Sb_x or the (110) plane for a CuPt-ordered (Ga,In)P along $[\bar{1}11]$ direction. A unified understanding is given for all these seemingly very different types of SLs and alloys as resulting from phonon mode mixing associated with either a structural or a certain form of modulation that breaks the

translational symmetry. In addition, InAs/InAs_{1-x}Sb_x and InAs/GaSb SLs are shown to exhibit qualitatively different spectroscopy signatures when probed from the (110) cleaved edge but not from the (001) growth plane.

Considerable variations between the InAs/InAs_{1-x}Sb_x SLs grown by different systems indicate that the structures are far from perfect, likely with considerable thickness and composition fluctuations at the interfaces. This study provides the basic understanding of the vibrational properties of this emerging material system, which provides a meaningful reference for applying Raman spectroscopy as a nondestructive characterization technique in the future study of this SL system.

ACKNOWLEDGMENTS

The work at UNCC, GT, and ASU is supported by ARO/MURI (Grant No. W911NF-10-1-0524, Dr. William Clark). Sandia National Laboratories is a multimission laboratory managed and operated by National Technology and Engineering Solutions of Sandia LLC, a wholly owned subsidiary of Honeywell International Inc. for the U.S.

Department of Energy's National Nuclear Security Administration under contract DE-NA0003525. Y. Z. thanks Dr. Andrew Norman of NREL for very helpful discussions and acknowledges the support of Bissell Distinguished Professorship at UNCC.

-
- [1] D. Zuo, R. Liu, D. Wasserman, J. Mabon, Z.-Y. He, S. Liu, Y.-H. Zhang, E. A. Kadlec, B. V. Olson, and E. A. Shaner, Direct minority carrier transport characterization of InAs/InAsSb superlattice nBn photodetectors, *Appl. Phys. Lett.* **106**, 071107 (2015).
- [2] Z.-D. Ning, S.-M. Liu, S. Luo, F. Ren, F. Wang, T. Yang, F.-Q. Liu, Z.-G. Wang, and L.-C. Zhao, Growth and characterization of InAs/InAsSb superlattices by metal organic chemical vapor deposition for mid-wavelength infrared photodetectors, *Mater. Lett.* **164**, 213 (2016).
- [3] B. Olson, L. Murray, J. Prineas, M. Flatté, J. Olesberg, and T. Boggess, All-optical measurement of vertical charge carrier transport in mid-wave infrared InAs/GaSb type-II superlattices, *Appl. Phys. Lett.* **102**, 202101 (2013).
- [4] E. A. Plis, M. N. Kutty, and S. Krishna, Passivation techniques for InAs/GaSb strained layer superlattice detectors, *Laser Photonics Rev.* **7**, 45 (2013).
- [5] G. Chen, A. Hoang, S. Bogdanov, A. Haddadi, P. Bijjam, B.-M. Nguyen, and M. Razeghi, Investigation of impurities in type-II InAs/GaSb superlattices via capacitance-voltage measurement, *Appl. Phys. Lett.* **103**, 033512 (2013).
- [6] N. Baril, S. Bandara, L. Hoeglund, N. Henry, A. Brown, C. Billman, P. Maloney, E. Nallon, M. Tidrow, and J. Pellegrino, Low operating bias InAs/GaSb strain layer superlattice LWIR detector, *Infrared Phys. Technol.* **70**, 58 (2015).
- [7] C. H. Grein, P. M. Young, M. E. Flatte, and H. Ehrenreich, Long wavelength InAs/InGaSb infrared detectors: Optimization of carrier lifetimes, *J. Appl. Phys.* **78**, 7143 (1995).
- [8] P. Manurkar, S. Ramezani-Darvish, B.-M. Nguyen, M. Razeghi, and J. Hubbs, High performance long wavelength infrared mega-pixel focal plane array based on type-II superlattices, *Appl. Phys. Lett.* **97**, 193505 (2010).
- [9] D. L. Smith and C. Mailhot, Proposal for strained type II superlattice infrared detectors, *J. Appl. Phys.* **62**, 2545 (1987).
- [10] E. R. Youngdale, J. R. Meyer, C. A. Hoffman, F. J. Bartoli, C. H. Grein, P. M. Young, H. Ehrenreich, R. H. Miles, and D. H. Chow, Auger lifetime enhancement in InAs-Ga_{1-x}In_xSb superlattices, *Appl. Phys. Lett.* **64**, 3160 (1994).
- [11] E. H. Steenbergen, B. C. Connelly, G. D. Metcalfe, H. Shen, M. Wraback, D. Lubyshev, Y. Qiu, J. M. Fastenau, A. W. K. Liu, S. Elhamri, O. O. Cellek, and Y. H. Zhang, Significantly improved minority carrier lifetime observed in a long-wavelength infrared III-V type-II superlattice comprised of InAs/InAsSb, *Appl. Phys. Lett.* **99**, 251110 (2011).
- [12] H. S. Kim, O. O. Cellek, Z.-Y. Lin, Z.-Y. He, X.-H. Zhao, S. Liu, H. Li, and Y.-H. Zhang, Long-wave infrared nBn photodetectors based on InAs/InAsSb type-II superlattices, *Appl. Phys. Lett.* **101**, 161114 (2012).
- [13] G. Belenky, G. Kipshidze, D. Donetsky, S. P. Svensson, W. L. Sarney, H. Hier, L. Shterengas, D. Wang, and Y. Lin, in *Infrared Technology and Applications*, edited by B. F. Andresen, G. F. Fulop, and P. R. Norton, SPIE Proceedings Vol. XXXVII (SPIE-International Society for Optical Engineering, Bellingham, WA, 2011).
- [14] S. P. Svensson, D. Donetsky, D. Wang, H. Hier, F. J. Crowne, and G. Belenky, Growth of type II strained layer superlattice, bulk InAs and GaSb materials for minority lifetime characterization, *J. Cryst. Growth* **334**, 103 (2011).
- [15] G. D. Mahan and J. O. Sofo, The best thermoelectric, *Proc. Natl. Acad. Sci. U.S.A.* **93**, 7436 (1996).
- [16] Y. Zhang, L.-W. Wang, and A. Mascarenhas, "Quantum coaxial cables" for solar energy harvesting, *Nano Lett.* **7**, 1264 (2007).
- [17] T. Bauer, *Thermophotovoltaics* (Springer, New York, 2011).
- [18] E. Plis, T. Schuler-Sandy, D. Ramirez, S. Myers, and S. Krishna, Dark current reduction in InAs/InAsSb superlattice mid-wave infrared detectors through restoration etch, *Electron. Lett.* **51**, 2009 (2015).
- [19] L. Höglund, D. Z. Ting, A. Khoshakhlagh, A. Soibel, C. J. Hill, A. Fisher, S. Keo, and S. D. Gunapala, Influence of radiative and non-radiative recombination on the minority carrier lifetime in midwave infrared InAs/InAsSb superlattices, *Appl. Phys. Lett.* **103**, 221908 (2013).
- [20] Y. Aytac, B. V. Olson, J. K. Kim, E. A. Shaner, S. D. Hawkins, J. F. Klem, J. Olesberg, M. E. Flatté, and T. F. Boggess, Bandgap and temperature dependence of Auger recombination in InAs/InAsSb type-II superlattices, *J. Appl. Phys.* **119**, 215705 (2016).
- [21] Y. Aytac, B. V. Olson, J. K. Kim, E. A. Shaner, S. D. Hawkins, J. F. Klem, M. E. Flatté, and T. F. Boggess, Evidence of a Shockley-Read-Hall Defect State Independent of Band-Edge Energy in InAs/In(As,Sb) Type-II Superlattices, *Phys. Rev. Applied* **5**, 054016 (2016).
- [22] B. V. Olson, J. F. Klem, E. A. Kadlec, J. K. Kim, M. D. Goldflam, S. D. Hawkins, A. Tauke-Pedretti, W. T. Coon, T. R. Fortune, E. A. Shaner, and M. E. Flatté, Vertical Hole Transport and Carrier Localization in InAs/InAs_{1-x}Sb_x Type-II Superlattice Heterojunction Bipolar Transistors, *Phys. Rev. Applied* **7**, 024016 (2017).
- [23] Y. T. Cherng, K. Y. Ma, and G. B. Stringfellow, Raman-scattering in InAs_{1-x}Sb_x grown by organometallic vapor-phase epitaxy, *Appl. Phys. Lett.* **53**, 886 (1988).
- [24] Y. B. Li, S. S. Dosanjh, I. T. Ferguson, A. G. Norman, A. G. Deoliveira, R. A. Stradling, and R. Zallen, Raman-scattering in InAs_{1-x}Sb_x alloys grown in GaAs by molecular-beam epitaxy, *Semicond. Sci. Technol.* **7**, 567 (1992).
- [25] D. Berdekas and S. Ves, Lattice dynamics and Raman scattering by phonons of GaAs/AlAs (001) superlattices, *J. Phys. Condens. Matter* **21**, 275405 (2009).
- [26] J. Menéndez, Phonons in GaAs-Al_xGa_{1-x}As superlattices, *J. Lumin.* **44**, 285 (1989).
- [27] H. Liu, N. Yue, Y. Zhang, P. Qiao, D. Zuo, B. Kesler, S. L. Chuang, J.-H. Ryou, J. D. Justice, and R. Dupuis, Lattice vibration modes in type-II superlattice InAs/GaSb with non-common-atom interface and overlapping vibration spectra, *Phys. Rev. B* **91**, 235317 (2015).
- [28] A. Fasolino, E. Molinari, and J. C. Maan, Calculated superlattice and interface phonons of InAs/GaSb superlattices, *Phys. Rev. B* **33**, 8889 (1986).

- [29] A. Fainstein, P. Etchegoin, M. P. Chamberlain, M. Cardona, K. Totemeyer, and K. Eberl, Selection rules and dispersion of GaAs/AlAs multiple-quantum-well optical phonons studied by Raman scattering in right-angle, forward, and backscattering in-plane geometries, *Phys. Rev. B* **51**, 14448 (1995).
- [30] R. Hessmer, A. Huber, T. Egeler, M. Haines, G. Tränkle, G. Weimann, and G. Abstreiter, Interface-phonon dispersion and confined-optical-mode selection rules of GaAs/AlAs superlattices studied by micro-Raman spectroscopy, *Phys. Rev. B* **46**, 4071 (1992).
- [31] B. Jusserand and M. Cardona, in *Light Scattering in Solids*, edited by M. Cardona and G. Güntherodt (Springer, Berlin, 1989), p. 49.
- [32] A. Mascarenhas, H. Cheong, and F. Alsina, in *Spontaneous Ordering in Semiconductor Alloys*, edited by A. Mascarenhas (Kluwer Academy, New York, 2002), p. 391.
- [33] F. Schäffler and G. Abstreiter, Electric-field-induced Raman scattering: Resonance, temperature, and screening effects, *Phys. Rev. B* **34**, 4017 (1986).
- [34] A. G. Norman, T. Y. Seong, I. T. Ferguson, G. R. Booker, and B. A. Joyce, Structural studies of natural superlattices in group III-V alloy epitaxial layers, *Semicond. Sci. Technol.* **8**, S9 (1993).
- [35] T. Y. Seong, A. G. Norman, I. T. Ferguson, and G. R. Booker, Transmission electron microscopy and transmission electron diffraction structural studies of heteroepitaxial InAs_ySb_{1-y} molecular-beam epitaxial layers, *J. Appl. Phys.* **73**, 8227 (1993).
- [36] H. M. Cheong, Y. Zhang, A. G. Norman, J. D. Perkins, A. Mascarenhas, K. Y. Cheng, and K. C. Hsieh, Resonance Raman scattering studies of composition-modulated GaP/InP short-period superlattices, *Phys. Rev. B* **60**, 4883 (1999).
- [37] R. L. Farrow, R. K. Chang, S. Mroczkowski, and F. H. Pollak, Detection of excess crystalline As and Sb in III-V oxide interfaces by Raman scattering, *Appl. Phys. Lett.* **31**, 768 (1977).
- [38] E. H. Steenbergen, Y. Huang, J. H. Ryou, L. Ouyang, J. J. Li, D. J. Smith, R. D. Dupuis, and Y. H. Zhang, Structural and optical characterization of type-II InAs/InAs_{1-x}Sb_x superlattices grown by metalorganic chemical vapor deposition, *Appl. Phys. Lett.* **99**, 071111 (2011).
- [39] E. H. Steenbergen, K. Nunna, L. Ouyang, B. Ullrich, D. L. Huffaker, D. J. Smith, and Y.-H. Zhang, Strain-balanced InAs/InAs_{1-x}Sb_x type-II superlattices grown by molecular beam epitaxy on GaSb substrates, *J. Vac. Sci. Technol. B* **30**, 02B107 (2012).
- [40] M. R. Wood, K. Kanedy, F. Lopez, M. Weimer, J. F. Klem, S. D. Hawkins, E. A. Shaner, and J. K. Kim, Monolayer-by-monolayer compositional analysis of InAs/InAsSb superlattices with cross-sectional STM, *J. Cryst. Growth* **425**, 110 (2015).
- [41] P. Yu and M. Cardona, *Fundamentals of Semiconductors* (Springer, New York, 2010).
- [42] A. Mascarenhas, *Spontaneous Ordering in Semiconductor Alloys* (Kluwer Academic/Plenum Publishers, New York, 2002).
- [43] B. Jusserand, P. Voisin, M. Voos, L. L. Chang, E. E. Mendez, and L. Esaki, Raman scattering in GaSb-AlSb strained layer superlattices, *Appl. Phys. Lett.* **46**, 678 (1985).
- [44] A. Fasolino, E. Molinari, and J. C. Maan, Resonant quasi-confined optical phonons in semiconductor superlattices, *Phys. Rev. B* **39**, 3923 (1989).
- [45] D. Berdekas and G. Kanellis, Phonon confinement in InAs/GaSb superlattices, *Phys. Rev. B* **43**, 9976 (1991).
- [46] F. Cerdeira, A. Pinczuk, J. C. Bean, B. Batlogg, and B. A. Wilson, Raman scattering from Ge_xSi_{1-x}/Si strained-layer superlattices, *Appl. Phys. Lett.* **45**, 1138 (1984).
- [47] H. K. Shin, D. J. Lockwood, and J. M. Baribeau, Strain in coherent-wave SiGe/Si superlattices, *Solid State Commun.* **114**, 505 (2000).
- [48] R. Loudon, Raman effect in crystals, *Adv. Phys.* **13**, 423 (1964).
- [49] A. K. Sood, J. Menéndez, M. Cardona, and K. Ploog, Resonance Raman Scattering by Confined LO and TO Phonons in GaAs-AlAs Superlattices, *Phys. Rev. Lett.* **54**, 2111 (1985).